Article

Discovery Medicine 2024; 36(183): 699–713
https://doi.org/10.24976/Discov.Med.202436183.66

Aminophylline Improves Ventilator-Induced Diaphragmatic Dysfunction by Targeting IGF-1-FOXO1-MURF1 Pathway

Luyu Yang[1,†], Xiaohong Jiang[2,†], Jinhui Tan[3], Shouzhi Fu[1,*], Wankang Dian[1,*]

[1]Department of ICU/Emergency, Wuhan Third Hospital & Tongren Hospital of Wuhan University, 430070 Wuhan, Hubei, China
[2]Department of Surgery, China University of Geosciences (Wuhan) Hospital, 430070 Wuhan, Hubei, China
[3]Department of Anesthesia, Wuhan Third Hospital & Tongren Hospital of Wuhan University, 430070 Wuhan, Hubei, China
*Correspondence: dwkljy@163.com (Wankang Dian); fszfsz181@163.com (Shouzhi Fu)
[†]These authors contributed equally.
Published: 20 April 2024

Background: The usage of life-saving mechanical ventilation (MV) could cause ventilator-induced diaphragmatic dysfunction (VIDD), increasing both mortality and morbidity. Aminophylline (AP) has the potential to enhance the contractility of animal skeletal muscle fibers and improve the activity of human respiratory muscles, and the insulin-like growth factor-1 (IGF-1)-forkhead box protein O1 (FOXO1)-muscle RING finger-1 (MURF1) pathway plays a crucial role in skeletal muscle dysfunction. This study aimed to investigate the impact of AP on VIDD and to elucidate the role of the IGF-1-FOXO1-MURF1 pathway as an underlying mechanism.

Methods: Rat models of VIDD were established through MV treatment. *IGF-1* lentiviral (LV) interference (LV-*IGF-1*-shRNA; controlled by lentiviral negative control LV-NC) was employed to inhibit *IGF-1* expression and thereby block the IGF-1-FOXO1-MURF1 pathway. Protein and mRNA levels of *IGF-1*, *FOXO1*, and *MURF1* were assessed using western blot and real-time reverse transcriptase-polymerase chain reaction (RT-qPCR), respectively. Diaphragm contractility and morphometry were examined through measurement of compound muscle action potentials (CMAPs) and hematoxylin and eosin (H&E) staining. Oxidative stress was evaluated by levels of hydrogen peroxide (H_2O_2), superoxide dismutase (SOD), antioxidant glutathione (GSH), and carbonylated protein. Mitochondrial stability was assessed by measuring the mitochondrial membrane potential (MMP), and mitochondrial fission and mitophagy were examined through protein levels of dynamin-related protein 1 (DRP1), mitofusin 2 protein (MFN2), phosphatase and tensin homolog (PTEN)-induced kinase 1 (PINK1), and Parkin (western blot). Apoptosis was evaluated using the terminal deoxynucleotidyl transferase-mediated uridine 5′-triphosphate (UTP) nick-end labeling (TUNEL) assay and levels of Bax, B-cell lymphoma 2 (*BCL-2*), and Caspase-3. Levels of Atrogin-1, neuronally expressed developmentally downregulated 4 (*NEDD4*), and muscle ubiquitin ligase of SCF complex in atrophy-1 (*MUSA1*) mRNA, as well as ubiquitinated protein, were utilized to determine protein degradation. Furthermore, the SUnSET (surface sensing of translation) method was employed to determine rates of protein synthesis.

Results: MV treatment upregulated *IGF-1* while downregulated *FOXO1* and *MURF1* ($p < 0.05$). AP administration reversed *IGF-1*, *FOXO1* and *MURF1* ($p < 0.05$), which was suppressed again by *IGF-1* inhibition ($p < 0.05$), demonstrating the blockage of the IGF-1-FOXO1-MURF1 pathway. MV treatment caused decreased CMAP and cross-sectional areas of diaphragm muscle fibers, and increased time course of CMAP ($p < 0.05$). Additionally, oxidative stress, cell apoptosis, and protein degradation were increased and mitochondrial stability was decreased by MV treatment ($p < 0.05$). Conversely, AP administration reversed all these changes induced by MV, but this reversal was disrupted by the blockage of the IGF-1-FOXO1-MURF1 pathway.

Conclusions: In this study, MV treatment induced symptoms of VIDD in rats, which were all effectively reversed by AP regulating the IGF-1-FOXO1-MURF1 pathway, demonstrating the potential of AP in ameliorating VIDD.

Keywords: aminophylline; ventilator-induced diaphragmatic dysfunction; *IGF-1*; *FOXO1*; *MURF1*; diaphragm

Introduction

Patients experiencing severe hypoxemic respiratory failure, unable to achieve sufficient alveolar ventilation, can fulfill the pulmonary gas exchange through mechanical ventilation (MV), a life-saving intervention [1,2]. Conversely, unsuccessful weaning from prolonged MV leads to extended hospitalization and is associated with elevated mortality and morbidity rates [3]. Prolonged or even short-term MV use can induce diaphragmatic weakness, characterized by diaphragmatic muscle atrophy and contractile dysfunction [1], thereby exerting deleterious effects on diaphragm structure and function [4].

The loss of contractility and muscle atrophy in the diaphragm resulting from MV is termed ventilator-induced diaphragmatic dysfunction (VIDD) and has been established to significantly correlate with difficulties in weaning from MV [5]. Incidence rates of VIDD and weaning challenges among MV-receiving patients have been reported at 63% and up to 35%, respectively [6]. Beyond increased mortality and morbidity, extended hospital stays, and weaning challenges, VIDD can give rise to complications such as pneumonia and a poor prognosis for critically ill patients [7].

Aminophylline (AP), a compound consisting of ethylenediamine and theophylline, has been demonstrated to possess bronchodilatory properties, enhance corticosteroid actions, control inflammation, and stimulate the respiratory neuronal network [8]. The theophylline component in AP has been proven to ameliorate chronic obstructive pulmonary disease (COPD), a condition associated with skeletal muscle atrophy and dysfunction [9]. Previous studies have showcased the supportive effects of AP in increasing the contractility of animal skeletal muscle fibers and enhancing the activity of human respiratory muscles [10]. Notably, acting as a significant agonist, AP has been reported to augment the shortening and contractility of the diaphragm, leading to increased ventilation [11].

Given that AP serves not only as a bronchodilator but also improves the function of the diaphragm and peripheral skeletal muscles, we hypothesized that AP could mitigate VIDD, a condition also associated with skeletal muscle weakness, atrophy, and dysfunction.

The insulin-like growth factor-1 (*IGF-1*) pathways, serving as regulators of both protein degradation and protein synthesis, play pivotal roles in influencing myofiber size and the function of skeletal muscles [12]. Simultaneously, muscle RING finger-1 (*MURF1*), a key E3 ubiquitin ligase in skeletal muscles responsible for mediating protein ubiquitination, is notably decreased during muscle atrophy [13]. It is essential to note that in models of muscle atrophy, *IGF-1* suppresses the transcription of *MURF1* through the class O-type forkhead transcription factors (*FOXOs*) [14]. Furthermore, forkhead box protein O1 (*FOXO1*) can activate and induce the expression of *MURF1*, while inhibiting *FOXO1* prevents the upregulation of *MURF1* expression and offers protection against muscle atrophy [15]. The interplay of these mechanisms related to protein catabolism and muscle atrophy underscores the critical roles of the IGF-1-FOXO1-MURF1 pathway in skeletal muscle dysfunction.

In this study, rat models of VIDD were established using MV treatment. The activation of the IGF-1-FOXO1-MURF1 pathway was modulated by introducing *IGF-1* lentiviral (LV) interference (LV-*IGF-1*-shRNA) to inhibit *IGF-1* expression in the rats. Building upon these rat models and employing AP, we assessed our hypothesis that AP exhibits ameliorative effects on VIDD, and this improvement occurs through the IGF-1-FOXO1-MURF1 pathway.

Materials and Methods

Animals

This study received approval from the Ethics Committee of Wuhan University (approval No. ZN2022057). Adult male Sprague-Dawley (SD) rats (n = 40), aged 8 weeks and weighing between 240–260 g, were procured from Beijing Vital River Laboratory Animal Technology Co., Ltd. (Beijing, China). Prior to the commencement of the study, rats were individually housed and acclimated for 1 week at a temperature of 26 ± 2 °C, under a standard 12-hour light/dark cycle, and provided with ample food and water.

The rats were divided into four groups (n = 10): rats in NC group were treated solely with lentiviral negative control (LV-NC), rats treated with LV-NC and subjected to MV (MV group), rats treated with LV-NC, MV, and AP (MV+AP group), and rats treated with LV inhibition of *IGF-1*, MV, and AP (MV+AP+LV-*IGF-1*-shRNA group).

Inhibition of IGF-1 by Lentiviral Interference

The *IGF-1* lentiviral interference (LV-*IGF-1*-shRNA; sense 5′-CCGGGCTCTTCAGTTCGTGTGTGGACTCGAGTCCACACACGAACTGAAGAGCTTTTTTG-3′, antisense 5′-AATTCAAAAAAGCTCTTCAGTTCGTGTGTGGACTCGAGTCCACACACGAACTGAAGAGC-3′) and negative control (LV-NC; sense 5′-CCGGTTCTCCGAACGTGTCACGTCTCGAGACGTGACACGTTCGGAGAATTTTTTG-3′, antisense 5′-AATTCAAAAAATTCTCCGAACGTGTCACGTCTCGAGACGTGACACGTTCGGAGAA-3′) were obtained from GeneChem (Order No. GOSE0336379, Shanghai, China). All rats underwent anesthesia with 1% sodium pentobarbital (P3761, Sigma-Aldrich, St. Louis, MO, USA) via intraperitoneal injection at doses of 40 mg/kg. Subsequently, LV interference (5 µL, 2 µg/µL) was delivered to the right ventricle using a microsyringe at a rate of 0.5 µL/min. Following a 14-day period post-injection, the remaining experiments were conducted.

Drug Administration and Mechanical Ventilation Treatment

In the MV+AP group and MV+AP+LV-*IGF-1*-shRNA group, each rat received a dose of 5 mg/kg of AP (HY-B0140, MedChemExpress, Monmouth Junction, NJ, USA) [16] administered through intraperitoneal injection. In contrast, for each rat in the Control group and MV group, an equivalent volume of normal saline (0.9% sodium chloride solution; ST341, Beyotime, Shanghai, China) was administered via intraperitoneal injection. The dose administrations were conducted for four consecutive days, consistently at the same time each day. On the fourth day, aseptic MV treatment surgery was performed, occurring two hours after the administration of normal saline/AP.

Two hours before anesthesia, rats received both the usual normal saline/AP and glycopyrrolate at a dosage of 0.04 mg/kg, administered intramuscularly. Subsequently, all rats were anesthetized via intraperitoneal injection of sodium pentobarbital (40 mg/kg). At two-hour intervals post-anesthesia, rats received intramuscular injections of glycopyrrolate (0.04 mg/kg). Following tracheostomy, rats were subjected to MV (SAR-830/AP, Quatronix, Beijing, China) for 18 hours, utilizing humidified air at 37 °C and O_2-enriched conditions. The tidal volume was set at 10 mL/kg based on individual body weight, with a respiratory rate of 80 breaths/minute and an expiration ratio of 1:2 [17]. Throughout the surgery, a nasogastric tube was employed for nutritional delivery, and rats were closely monitored at a temperature of 37 $\pm$ 0.5 °C.

Puromycin Administration

The administration of puromycin was carried out for the subsequent assessment of protein synthesis. At 24 hours after the MV treatment surgery, all rats received intraperitoneal injections of a carefully prepared stock solution of puromycin. The dosage criterion was set at 40 nmol/g of individual weight, and each rat was injected with a volume of 80–120 µL of the stock solution [18]. Subsequently, the rats were returned to their cages and maintained appropriately for a duration of 30 minutes.

The Detection of Non-Invasive Compound Muscle Action Potentials (CMAPs)

At the conclusion of the 30-minute period following puromycin administration, CMAPs were measured. To achieve this, rats were anesthetized with 1% sodium pentobarbital (P3761, Sigma-Aldrich, St. Louis, MO, USA) via intraperitoneal injection at doses of 40 mg/kg. The depth of anesthesia was assessed and verified through pedal and blink reflexes. Throughout the surgery, heart rate and respiratory rate were monitored to prevent fluctuations, and the rats' eyes were treated with veterinary ointment to prevent dryness.

A subcutaneous acupuncture needle was inserted into the proximal tail as a ground electrode. Another acupuncture needle, serving as the reference electrode, was inserted into the contralateral abdomen. The recording electrode, in the form of an electrode sheet, was attached to the lower edge of the ipsilateral rib. Two additional acupuncture needles, acting as stimulating electrodes, were inserted vertically above the same side of the clavicle, positioned 0.5 cm away from the trachea. All acupuncture needles were inserted to a depth of 1 cm, maintaining a distance of 0.5 cm between two acupuncture needles. The red and black stimulation connectors were respectively connected to the near-heart end and the telecentric end. Stimulation involved a single positive voltage pulse (4–6 V) with 30-second intervals. Parameters such as wave width (1 ms) and delay (1 ms) were set. The CMAP was recorded using a physiological signal system (RM6240, ChengYi, Chengdu, China). The average response of each rat was obtained by applying stimulation three times consecutively.

Sample Collection

Following the measurement of CMAPs, rats were administered with 1% sodium pentobarbital (P3761, Sigma-Aldrich, St. Louis, MO, USA) via intraperitoneal injection at doses of 180 mg/kg. Euthanasia was ensured through a thoracotomy to observe cardiac and respiratory arrest. Subsequently, the diaphragm of each rat was harvested. The costal diaphragm from each diaphragm was used to isolate mitochondria. A diaphragm segment from each rat was specifically prepared for the terminal deoxynucleotidyl transferase-mediated uridine 5′-triphosphate (UTP) nick-end labeling (TUNEL) assay.

Briefly, the diaphragm segment was initially placed in cold PBS, then transferred to 4% paraformaldehyde (in PBS) at 4 °C for 1 day, followed by transfer into 30% sucrose (in PBS) at 4 °C for 1 day. The tissues were subsequently embedded in an optimal cutting temperature (OCT) embedding medium and stored at –80 °C. The remaining diaphragm was snap-frozen in liquid nitrogen and directly stored at –80 °C.

Cross-Sectional Areas (CSAs) of Muscle Fiber

Segments of each diaphragm from each rat were immersed in an alcohol-formol bath, fixed in 10% paraformaldehyde, and subsequently embedded in paraffin. The paraffin-embedded diaphragm tissues were then sliced into sections with a thickness of 6 µm and stained with hematoxylin (C0107, Beyotime, Shanghai, China) and eosin (C0109, Beyotime, Shanghai, China). The morphometric examination of muscle fibers was conducted using an optical microscope (Olympus CK31, Olympus, Tokyo, Japan), and the cross-sectional areas were measured and corrected using a factor of 1.53 (the specific correction factor for the diaphragm [19]).

Determination of Oxidative Stress Levels

Diaphragm tissues were lysed using pre-cooled radioimmunoprecipitation assay (RIPA) lysis buffer (P0013D, Beyotime, Shanghai, China), homogenized, and centrifuged at 3000 rpm/min for 15 minutes. The collected supernatants were analyzed using commercially obtained assay kits, following the manufacturers' instructions, to determine the levels of hydrogen peroxide (H_2O_2) (ab102500, Abcam, Cambridge, MA, USA), superoxide dismutase (SOD; S0101S, Beyotime, Shanghai, China), and antioxidant glutathione (GSH; E-EL-0026c, Elabscience Biotechnology Co., Ltd., Wuhan, China). Additionally, the levels of carbonylated protein were assessed using western blot, as described in the "western blot" section.

Detection of Mitochondrial Membrane Potential (MMP)

Following the manufacturer's instructions, a mitochondria isolation kit for tissues was utilized to extract mitochondrial proteins, cytoplasmic proteins, and mitochondria from the segments of the costal diaphragms from each rat. The JC-1 fluorescent probe (C2006, Beyotime, Shanghai, China) was employed to measure the MMPs. Under the fluorescence microscope (CKX53, Olympus, Tokyo, Japan), JC-1 would aggregate in the mitochondrial matrix and produce red fluorescence when MMP was high, while JC-1 would act as a monomer and produce green fluorescence when MMP was low. The quantification of red and green fluorescence was performed using Image J software (1.48, National Institutes of Health, Rockville, MD, USA), and the level of MMP was expressed by the ratio of JC-1 aggregates (red)/JC-1 monomers (green).

Measurement of Mitochondrial Fission and Mitophagy

The assessment of mitochondrial fission was conducted by measuring protein levels of dynamin-related protein 1 (DRP1), an essential protein during mitochondrial fission, and mitofusin 2 protein (MFN2), an essential protein for the stability of mitochondria. The level of mitophagy was evaluated by measuring protein levels of induced kinase 1 (PINK1) and Parkin, which are considered significant for the regulation of mitophagy. All these protein measurements were carried out using the western blot assay, as described in the "western blot" section.

Measurement of Apoptosis in Diaphragmatic Muscles

The apoptosis in muscles was initially determined by the TUNEL assay. Tissue molds prepared for the TUNEL assay were retrieved from –80 °C and sliced into sections of 8–10 µm. At least two sections from each sample were placed on a microscope slide and allowed to reach room temperature. The slides with sections were thoroughly washed with PBS (pH 7.4) and permeabilized with 0.2% Triton X-100 (T8200, Solarbio, Beijing, China) for 5 minutes. According to the manufacturer's instructions, the sections were subsequently treated using the TUNEL assay kit (C1088, Beyotime, Shanghai, China). Slides were then stained with DAPI (C1002, Beyotime, Shanghai, China) and visualized under a microscope (CKX53, Olympus, Tokyo, Japan). The average number of TUNEL-positive cells from three random regions was used for quantifying apoptosis.

Measurement of Protein Degradation in Diaphragmatic Muscle

The levels of protein degradation in diaphragm muscles from different groups were assessed using real-time reverse transcriptase-polymerase chain reaction (RT-qPCR) to measure mRNA levels of Atrogin-1/muscle atrophy F-box (*MAFbx*), neuronally expressed developmentally downregulated 4 (*NEDD4*), and muscle ubiquitin ligase of SCF complex in atrophy-1 (*MUSA1*), as described in the "RT-qPCR" section. Additionally, levels of protein ubiquitination were employed to evaluate protein degradation and obtained through western blot, as detailed in the "western blot" section.

Measurement of Protein Synthesis in Diaphragmatic Muscle

The measurement of protein synthesis was conducted using the non-radioactive, puromycin-based method known as the SUnSET (surface sensing of translation) assay. Given that rats were administered puromycin 30 minutes before euthanasia, protein synthesis was assessed through a western blot to detect the intensity of puromycin incorporation into newly synthesized protein peptides, as detailed in the "western blot" section.

Real-Time Reverse Transcriptase-Polymerase Chain Reaction

Total RNA was extracted from diaphragm tissues using the TRIzol® kit (DP424, Tiangen, Beijing, China). The supernatant containing RNAs was collected, and the RNAs were reverse-transcribed into cDNA using the FastQuant cDNA kit (KR116, Tiangen, Beijing, China). Primers for the target genes are listed in Table 1, and these target genes were amplified using the PCR instrument (LightCycler96, Roche, Shanghai, China). The method of $2^{-\Delta\Delta Cq}$ was employed for data analysis, with glyceraldehyde-3-phosphate dehydrogenase (*GAPDH*) used as the internal reference.

Western Blot

The diaphragm tissues were treated with RIPA lysis buffer (P0013D, Beyotime, Shanghai, China). Protein concentrations were determined using the bicinchoninic acid (BCA) assay kit (P0010S, Beyotime, Shanghai, China). Proteins were separated on a standard sodium dodecyl-

Table 1. Primer sequences.

Name	Sequence (5′-3′)
IGF-1-F	GCACTCTGCTTGCTCACCTTTA
IGF-1-R	TCCGAATGCTGGAGCCATA
FOXO1-F	GGGTTAGTGAGCAGGTTACAC
FOXO1-R	TCCAATGGCACAGTCCTTAT
MURF1-F	TGGCCCCATTGCAGAGTGTCTT
MURF1-R	TCCTTGGTCACTCGACGGGAAT
Bax-F	CCAAGAAGCTGAGCGAGTGT
Bax-R	CCGGAGGAAGTCCAATGTC
BCL-2-F	TCGCCCTGTGGATGACTGA
BCL-2-R	CAGAGACAGCCAGGAGAAATCA
Caspase-3-F	ATGGAGAACAACAAAACCTCAGT
Caspase-3-R	TTGCTCCCATGTATGGTCTTTAC
Atrogin-1-F	AGCTTGTGCGATGTTACCCA
Atrogin-1-R	GGTGAAAGTGAGACGGAGCA
NEDD4-F	TTGTCACTGGCACATCTCGGGT
NEDD4-R	TTGGCAGCTTTTCAGGAGTACCCC
MUSA1-F	GTGATCATGCCAATCCACAG
MUSA1-R	CATGAATGTCACCATGCACA
GAPDH-F	GGTGGTCTCCTCTGACTTCAACA
GAPDH-R	GTTGCTGTAGCAAATTCGTTGT

IGF-1, insulin-like growth factor-1; *FOXO1*, forkhead box protein O1; *MURF1*, muscle RING finger-1; *BCL-2*, B-cell lymphoma 2; *NEDD4*, neuronally expressed developmentally downregulated 4; *MUSA1*, muscle ubiquitin ligase of SCF complex in atrophy-1; *GAPDH*, glyceraldehyde-3-phosphate dehydrogenase; F, forward; R, reverse.

sulfate polyacrylamide gel electrophoresis (SDS-PAGE) gel (10%; P0937, Beyotime, Shanghai, China) and transferred to a polyvinylidene fluoride (PVDF) membrane (IPVH00010, Millipore Sigma, Billerica, MA, USA). Membranes were incubated with primary antibodies: anti-IGF-1 (1:2000 dilution, ab133542, Abcam, Cambridge, MA, USA), anti-FOXO1 (1:1000 dilution, 82358, Invitrogen, Carlsbad, CA, USA), anti-MURF1 (1:1000 dilution, PA5-76695, Invitrogen, Carlsbad, CA, USA), anti-2,4-Dinitrophenol (DNP; for detecting carbonylated protein; 1:1000 dilution, ab178020, Abcam, Cambridge, MA, USA), anti-DRP1 (1:1000 dilution, ab184247, Abcam, Cambridge, MA, USA), anti-MFN2 (1:2000, ab205236, Abcam, Cambridge, MA, USA), anti-PINK1 (1:1000 dilution, ab216144, Abcam, Cambridge, MA, USA), anti-Parkin (1:2000 dilution, ab77924, Abcam, Cambridge, MA, USA), anti-ubiquitin (1:1000 dilution, ab140601, Abcam, Cambridge, MA, USA), and anti-β-actin (1:2000 dilution, ab8224, Abcam, Cambridge, MA, USA).

After washing the membranes twice with tris buffered saline with tween (TBST; P0233, Beyotime, Shanghai, China) for 10 minutes each time, the membranes were incubated with horseradish peroxidase (HRP)-conjugated secondary antibody (1:2000 dilution, ab288151, Abcam, Cambridge, MA, USA) for 1 hour at room temperature. Protein bands were visualized using enhanced chemiluminescence (ECL; P0018, Beyotime, Shanghai, China). Images were processed with Adobe PhotoShop CS3 (Adobe Systems Inc., San Jose, CA, USA), and gray analysis was performed using AlphaEaseFC 4.0 (Alpha Innotech., San Leandro, CA, USA).

Statistical Analysis

The data were expressed as mean $\pm$ standard deviation (SD). Statistical analyses were conducted using GraphPad Prism 8.0.2 (GraphPad Software Inc., San Diego, CA, USA), and the significance of differences between groups was determined using Student's *t*-test or analysis of variance (ANOVA) followed by the post hoc Tukey's test. A significance level of $p < 0.05$ was considered statistically significant.

Results

Aminophylline Regulates IGF-1-FOXO1-MURF1 Pathway and Plays Roles in VIDD

Based on the mRNA expression shown in Fig. 1A and protein expression shown in Fig. 1B, MV treatment (the MV group) significantly decreased *IGF-1* and increased *FOXO1* and *MURF1* ($p < 0.05$), indicating the involvement of the IGF-1-FOXO1-MURF1 pathway in MV-induced VIDD. Rats treated with both MV and AP exhibited a significant increase in *IGF-1* expression and a decrease in *FOXO1* and *MURF1* expressions compared to rats treated only with MV ($p < 0.05$), suggesting that AP could modulate the IGF-1-FOXO1-MURF1 pathway and might impact VIDD. However, in the MV+AP+LV-*IGF-1*-shRNA group, where rats were treated with both MV and AP but *IGF-1* was inhibited, leading to the blockade of the IGF-1-FOXO1-MURF1 pathway, the *IGF-1* expression decreased, and *FOXO1* and *MURF1* expressions increased ($p < 0.05$). This demonstrates the disruption of IGF-1-FOXO1-MURF1 pathway activation.

AP Improves the Neuromuscular Electrophysiology and Diaphragm Fiber Cross-Sectional Areas (CSAs)

As depicted in Fig. 2A,B, MV treatment significantly decreased CMAP and increased the time course of CMAP compared with the NC group ($p < 0.05$). In the MV+AP group, AP administration significantly increased CMAP and decreased the time course of CMAP compared with the MV group ($p < 0.05$). However, when *IGF-1* was inhibited in the MV+AP+LV-*IGF-1*-shRNA group, CMAP significantly decreased, and the time course of CMAP significantly increased compared with the MV+AP group ($p < 0.05$).

Additionally, Fig. 2C shows that CSAs were significantly decreased in the MV group ($p < 0.05$) and were then increased by AP administration in the MV+AP group ($p <$

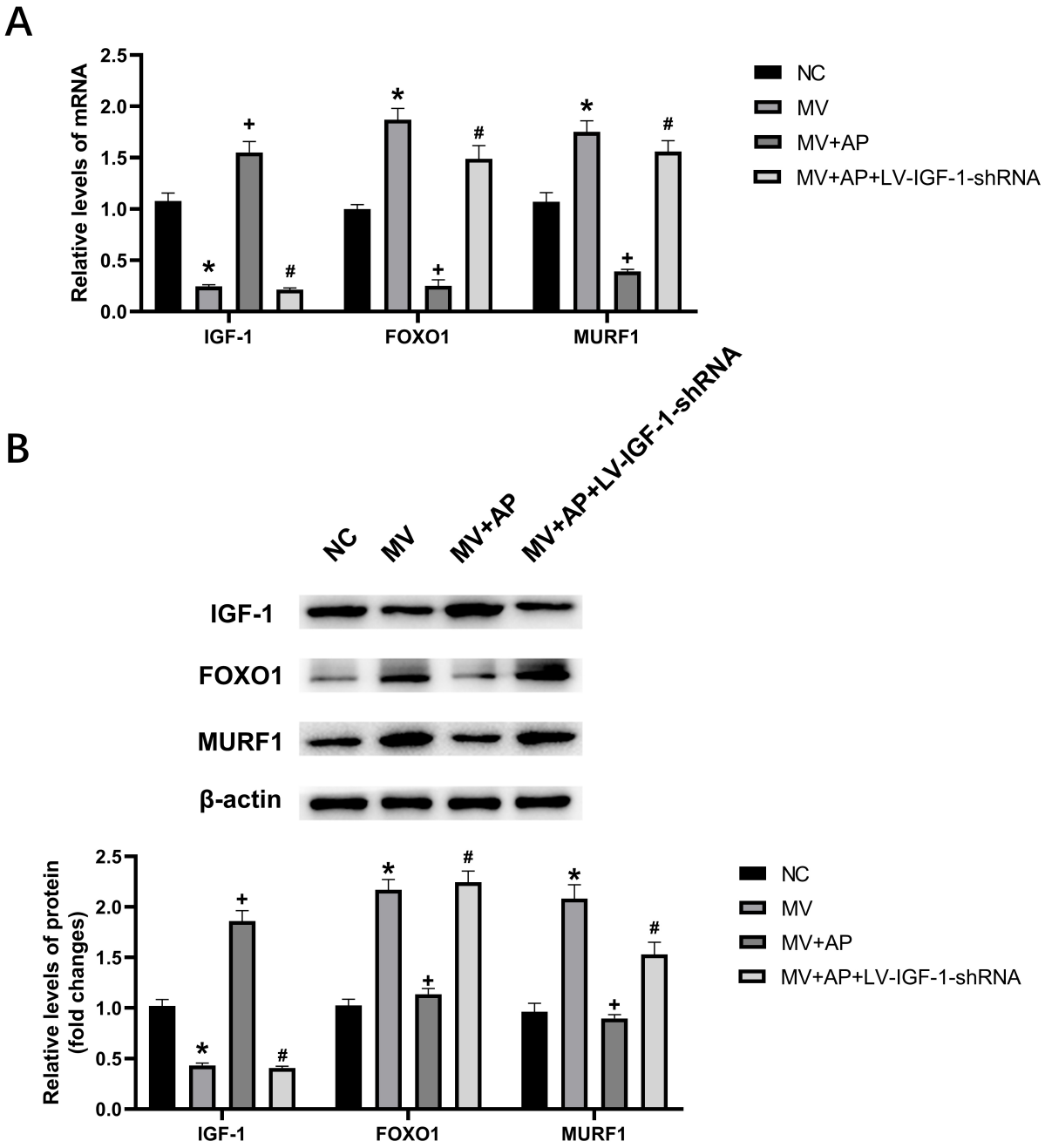

Fig. 1. Aminophylline (AP) regulates the IGF-1-FOXO1-MURF1 pathway and plays roles in ventilator-induced diaphragmatic dysfunction (VIDD). (A) Levels of *IGF-1*, *FOXO1*, *MURF1* mRNA expressions in diaphragms. (B) Levels of IGF-1, FOXO1, MURF1 protein expressions in diaphragms. N = 10. $^{*}p < 0.05$ compared with the NC group. $^{+}p < 0.05$ compared with the mechanical ventilation (MV) group. $^{\#}p < 0.05$ compared with MV+AP group.

0.05). However, in the MV+AP+*IGF-1* group, CSAs were significantly decreased compared with the MV+AP group ($p < 0.05$).

AP Ameliorates Oxidative Stress in Diaphragmatic Muscles

As illustrated in Fig. 3A,B, the contents of SOD and GSH significantly decreased in the MV group compared with the NC group ($p < 0.05$) and significantly increased in the MV+AP group compared with the MV group ($p < 0.05$). Furthermore, compared with the MV+AP group, the inhibition of *IGF-1* in the MV+AP+LV-*IGF-1*-shRNA group significantly decreased the contents of SOD and GSH ($p < 0.05$).

Additionally, Fig. 3C,D demonstrate that the content of H_2O_2 and the level of carbonylated protein significantly

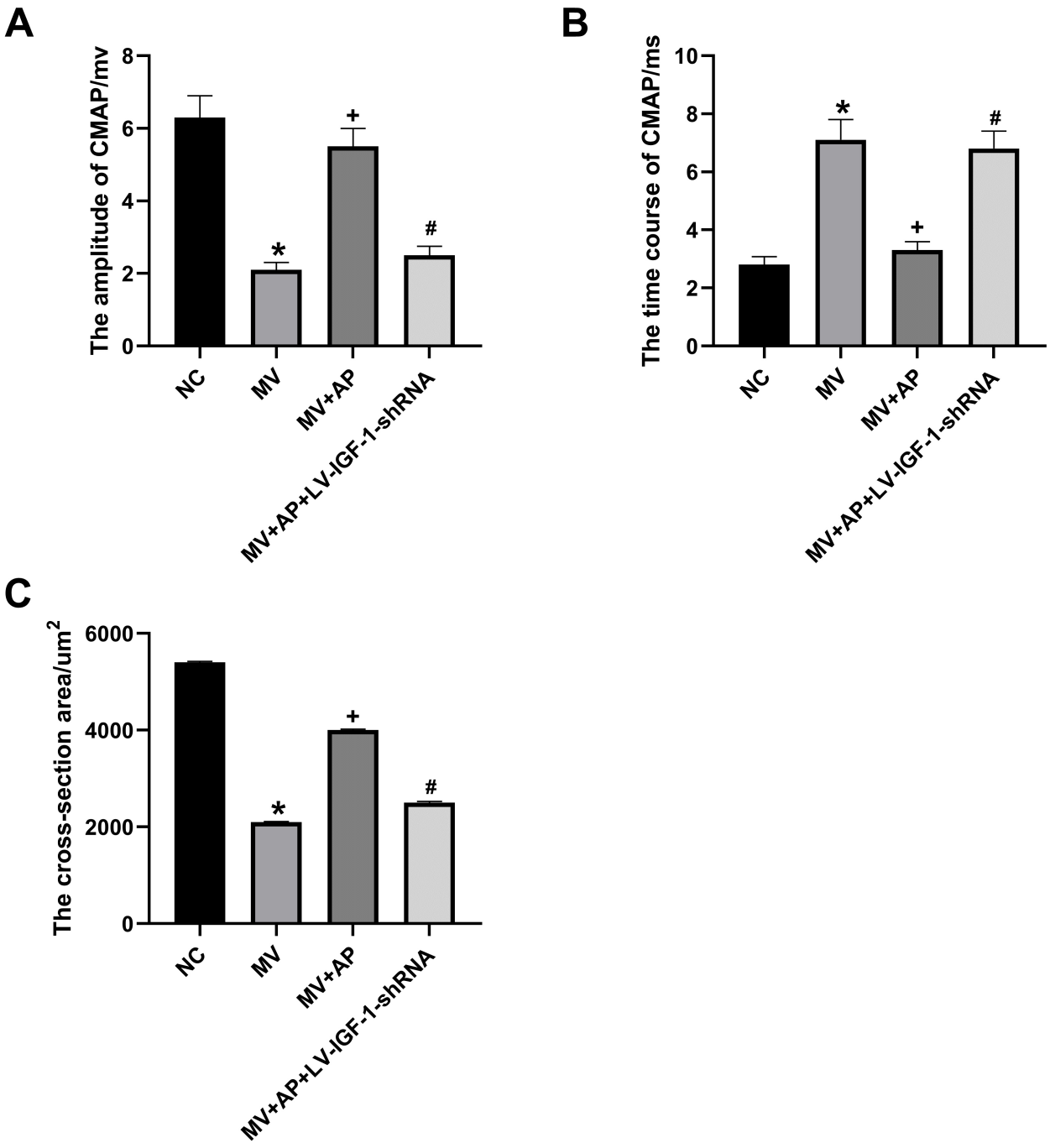

Fig. 2. AP improves the neuromuscular electrophysiology and diaphragm fiber cross-sectional areas (CSAs). (A) The amplitudes of compound muscle action potentials (CMAPs) of diaphragms. (B) The time courses of CMAP of diaphragms. (C) The quantification of cross-sectional areas. N = 10. *$p < 0.05$ compared with the NC group. $^{+}p < 0.05$ compared with the MV group. $^{\#}p < 0.05$ compared with MV+AP group.

increased in the MV group compared with the NC group ($p < 0.05$) and significantly decreased in the MV+AP group compared with the MV group ($p < 0.05$). Furthermore, compared with the MV+AP group, the content of H_2O_2 and the level of carbonylated protein significantly increased in the MV+AP+LV-*IGF-1*-shRNA group ($p < 0.05$).

AP Restores the Mitochondrial Membrane Potential and Improves Mitophagy in Diaphragmatic Muscles

As depicted in Fig. 4A, the ratio of JC-1 aggregates/JC-1 monomers significantly decreased in the MV group compared with the NC group ($p < 0.05$), indicating a decreased level of MMP. This ratio signifi-

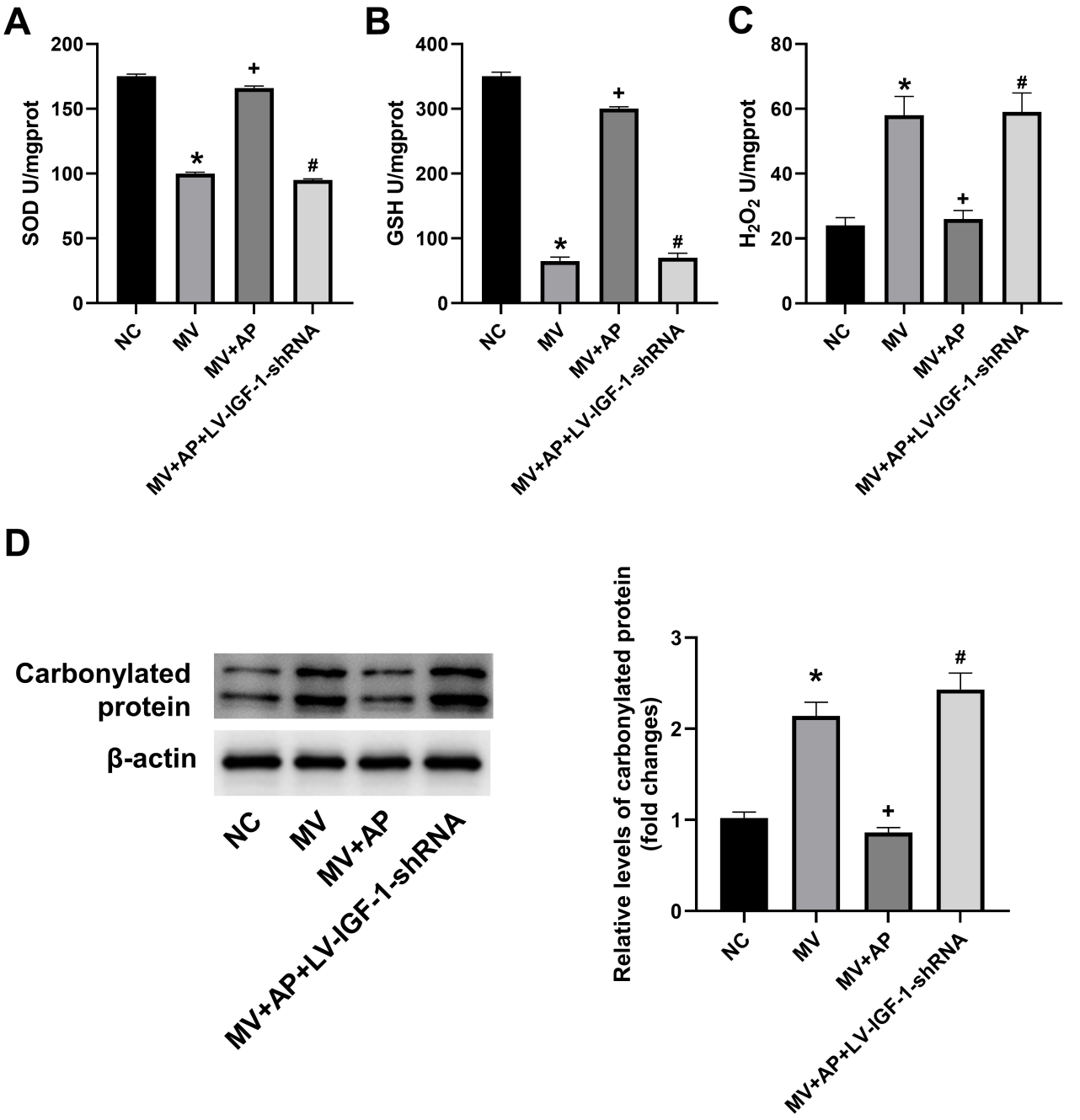

Fig. 3. AP ameliorates oxidative stress in diaphragmatic muscles. The levels of (A) superoxide dismutase (SOD), (B) antioxidant glutathione (GSH) and (C) hydrogen peroxide (H_2O_2) content in diaphragm tissues. (D) The carbonylated protein levels in diaphragm muscles. N = 10. *$p < 0.05$ compared with the NC group. $^{+}p < 0.05$ compared with the MV group. $^{\#}p < 0.05$ compared with MV+AP group.

cantly increased in the MV+AP group compared with the MV group ($p < 0.05$), indicating a higher level of MMP. Furthermore, compared with the MV+AP group, the inhibition of *IGF-1* in the MV+AP+LV-IGF-1-shRNA group significantly decreased the ratio of JC-1 aggregates/JC-1 monomers ($p < 0.05$).

Additionally, Fig. 4B,C show that the protein levels of DRP1, PINK1, and Parkin significantly increased, while the protein level of MFN2 significantly decreased in the MV group compared with the NC group ($p < 0.05$). These changes were significantly reversed in the MV+AP group compared with the MV group ($p < 0.05$). Furthermore, compared with the MV+AP group, the protein levels of DRP1, PINK1, and Parkin significantly increased, while the protein level of MFN2 significantly decreased in the MV+AP+LV-*IGF-1*-shRNA group ($p < 0.05$).

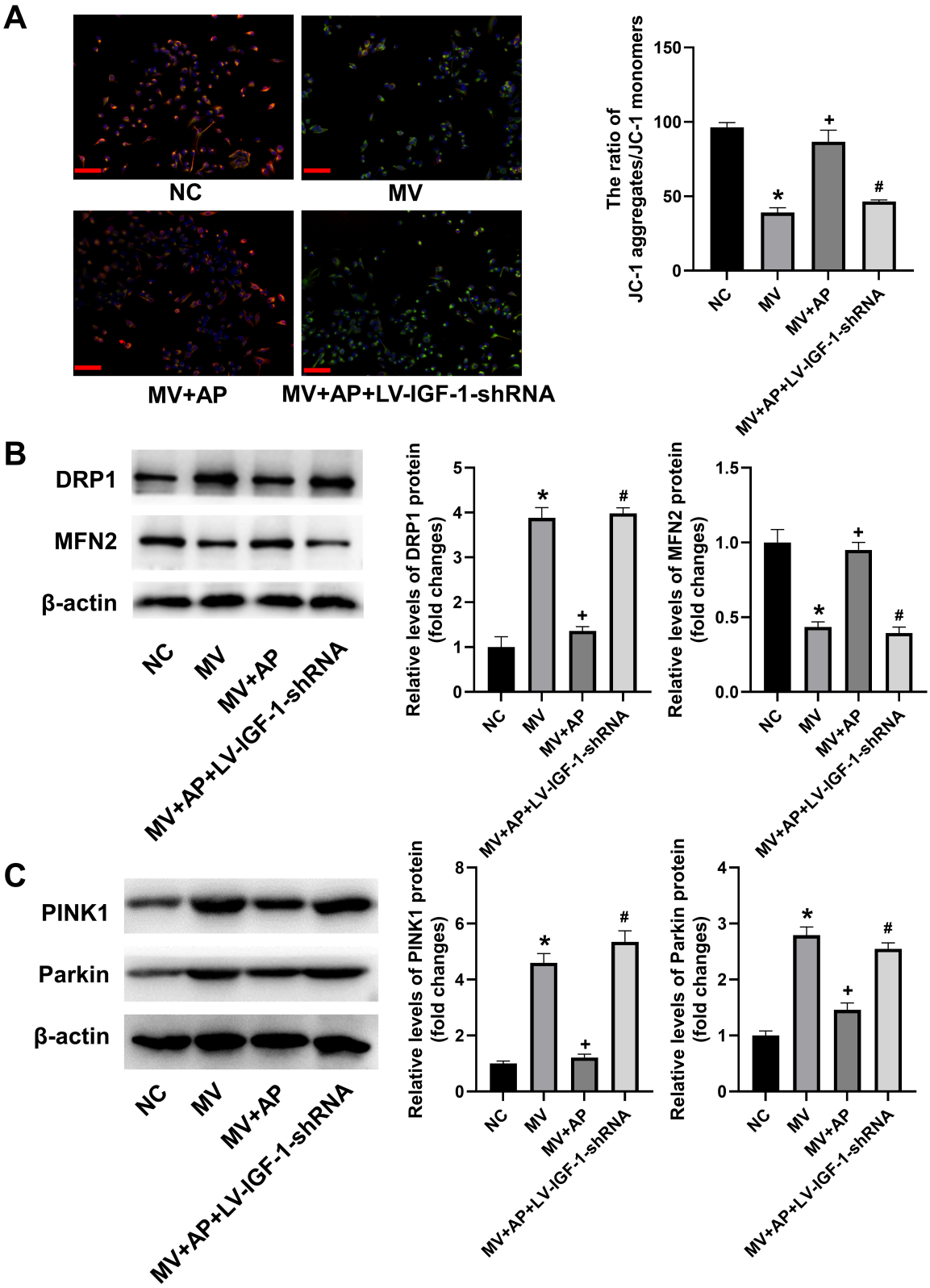

Fig. 4. AP restores the mitochondrial membrane potential (MMP) and ameliorates the mitophagy in diaphragmatic muscles. (A) Representative JC-1 fluorescence images for detecting MMP and the fluorescence quantification of MMP. Scale bar = 50 µm. Levels of protein expression of (B) dynamin-related protein 1 (DRP1) and mitofusin 2 protein (MFN2), and (C) phosphatase and tensin homolog (PTEN)-induced kinase 1 (PINK1) and Parkin in diaphragm tissues. N = 10. $^{*}p < 0.05$ compared with the NC group. $^{+}p < 0.05$ compared with the MV group. $^{\#}p < 0.05$ compared with MV+AP group.

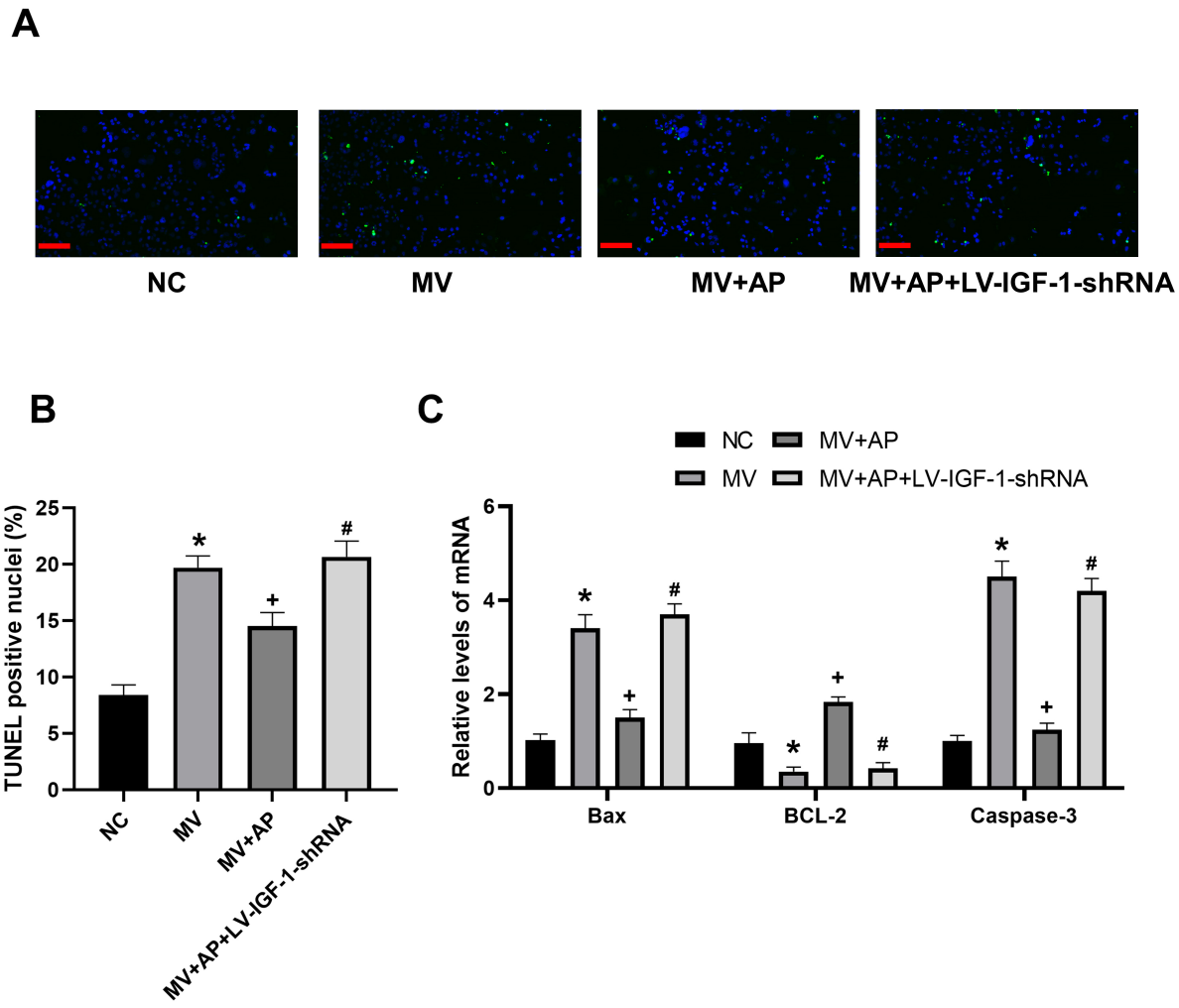

Fig. 5. AP ameliorates apoptosis in diaphragmatic muscles. (A) Representative images of terminal deoxynucleotidyl transferase-mediated uridine 5′-triphosphate (UTP) nick-end labeling (TUNEL) assay performed on diaphragms from differently treated rats. Scale bar = 50 µm. (B) The quantification of positively stained nuclei in the TUNEL assay for diaphragms. (C) The mRNA levels of Bax, *BCL-2* and Caspase-3. N = 10. $^{*}p < 0.05$ compared with the NC group. $^{+}p < 0.05$ compared with the MV group. $^{\#}p < 0.05$ compared with MV+AP group.

AP Ameliorates Apoptosis in Diaphragmatic Muscles

The results of the TUNEL assay, as depicted in Fig. 5A,B, demonstrated that the percentage of TUNEL-positive nuclei increased due to MV treatment ($p < 0.05$) in the MV group, while it was reversed by AP administration in the MV+AP group ($p < 0.05$). However, when *IGF-1* was inhibited, the TUNEL-positive nuclei and consequently apoptosis increased ($p < 0.05$).

Furthermore, Fig. 5C shows that the mRNA levels of Bax and Caspase-3 increased ($p < 0.05$), while the level of B-cell lymphoma 2 (*BCL-2*) decreased ($p < 0.05$) in the MV group. These changes were all reversed by AP administration in the MV+AP group ($p < 0.05$). Conversely, the decreased Bax and Caspase-3 and the increased *BCL-2* in the MV+AP group were all oppositely regulated in the MV+AP+LV-*IGF-1*-shRNA group ($p < 0.05$).

AP Suppresses Protein Degradation and Promotes Protein Synthesis in Diaphragmatic Muscles

Protein degradation and synthesis were assessed by examining related markers illustrated in Fig. 6. Using RT-qPCR, levels of Atrogin-1 (Fig. 6A), *NEDD4* (Fig. 6B), and *MUSA1* (Fig. 6C) were found to be upregulated after MV treatment ($p < 0.05$) in the MV group, while these upregulations were reversed by AP ($p < 0.05$) in the MV+AP group. Moreover, the decreased mRNA expressions increased again after *IGF-1* was inhibited ($p < 0.05$) in the MV+AP+LV-*IGF-1*-shRNA group.

Fig. 6D shows that protein ubiquitination increased in the MV group ($p < 0.05$), which was reversed in the MV+AP group ($p < 0.05$). Compared with the MV+AP group, protein ubiquitination in the MV+AP+LV-*IGF-1*-shRNA group increased again ($p < 0.05$).

The rate of protein synthesis was measured by detecting the amplitude of puromycin incorporated into newly synthesized proteins within a certain time (30 minutes). As shown in Fig. 6E, the level of puromycin detected in total diaphragm proteins in the MV group significantly decreased compared with that in the NC group ($p < 0.05$), indicating a decreased rate of protein synthesis. After AP administration, the level of puromycin increased significantly compared with the MV group ($p < 0.05$). Moreover, compared with the MV+AP group, the level of puromycin decreased significantly in the MV+AP+LV-*IGF-1*-shRNA group, where *IGF-1* was inhibited ($p < 0.05$).

Discussion

As a common and undesired consequence of MV treatment, VIDD is characterized by the rapid development of inspiratory muscle weakness, resulting from both diaphragmatic contractile dysfunction and atrophy [20,21]. VIDD, primarily driven by increased proteolysis of respiratory muscles, has been demonstrated to be associated with numerous mechanisms and cellular processes, including muscle atrophy, oxidative stress, structural injury, muscle fiber remodeling, mitochondrial energy deficiency, autophagy, and apoptosis [19].

In this study, we utilized established VIDD rat models to explore the effects of AP on ameliorating VIDD. We investigated how AP improves the mechanisms and cellular processes associated with VIDD.

In the present study, MV treatment was observed to decrease *IGF-1* expression while increasing the expressions of *FOXO1* and *MURF1* ($p < 0.05$). These MV-induced changes were subsequently reversed with the administration of AP ($p < 0.05$). These results affirm, as previously suggested, that the IGF-1-FOXO1-MURF1 pathway plays a crucial role in VIDD. They also suggest that AP has the potential to reverse the development of VIDD, and this reversal is associated, at least partially, with the IGF-1-FOXO1-MURF1 pathway.

Furthermore, the results obtained from the MV+AP+LV-*IGF-1*-shRNA group, focusing on the expressions of *IGF-1*, *FOXO1*, and *MURF1*, demonstrated that the effect of AP in reversing VIDD was not achieved when the IGF-1-FOXO1-MURF1 pathway failed to be activated. This finding verifies that AP affects VIDD, at least partially, by targeting the IGF-1-FOXO1-MURF1 pathway.

The CMAP, serving as a novel and non-invasive neurophysiological tool, records the electrical activities of muscles in response to transcutaneous stimulation of motor nerves [22]. The CMAP presents the summated action potentials of all stimulated motor endplates and is considered an objective neurophysiological parameter for assessing neuromuscular disorders, muscle hypertrophy and atrophy, and muscle contractions [23]. Previous reports indicate that CMAP examination can be utilized to assess motor unit loss in muscles. In comparison to traditional motor unit number estimation (MUNE) techniques, CMAP scanning offers numerous advantages, being automated, non-invasive, and achievable within minutes [24].

In this study, CMAP significantly decreased ($p < 0.05$), and the time course of CMAP significantly increased ($p < 0.05$) in the MV group, indicating damage to the motor unit caused by MV. However, after treatment with AP, both the decreased CMAP and increased time course of CMAP were reversed ($p < 0.05$). This demonstrates that AP is capable of improving the motor unit in the diaphragm damaged by MV usage and, consequently, enhancing the contractile function of the diaphragm in VIDD.

Furthermore, the proof that AP functions by activating the IGF-1-FOXO1-MURF1 pathway is supported by the results of the MV+AP+LV-*IGF-1*-shRNA group. In this group, compared to the MV+AP group, CMAP decreased ($p < 0.05$), and the time course of CMAP increased ($p < 0.05$) when the activation of the IGF-1-FOXO1-MURF1 pathway was blocked, even though AP was administered. A similar scenario occurred in the muscle fiber structure, where MV treatment induced a significant decrease in CSAs of diaphragmatic muscle fibers ($p < 0.05$), while AP treatment restored the CSAs ($p < 0.05$). However, blocking the IGF-1-FOXO1-MURF1 pathway resulted in a decrease in CSAs ($p < 0.05$) once again, emphasizing the critical role of the IGF-1-FOXO1-MURF1 pathway as the target for AP in restoring CSAs.

Given the dense packing of mitochondria in skeletal muscles due to their high metabolic demand, a significant amount of reactive oxygen species (ROS) is produced in muscles after damage, a factor considered crucial for muscle functions. It has been established that ROS, primarily originating from mitochondria in the diaphragm, contributes to mitochondrial oxidative stress (MOS), playing a key role in promoting protein degradation and exacerbating VIDD [25,26]. Additionally, oxidative stress is known to activate a feedback loop with ROS, promoting autophagy, thereby creating a cycle of increased ROS generation and elevated autophagy levels [27]. The mitochondrial membrane potential (MMP), would be decreased in response to ROS, leading to the translocation of Parkin to damaged mitochondria [28].

In this study, we confirmed the association between increased oxidative stress in muscles and MV-induced VIDD. MV treatment resulted in a decrease SOD and GSH contents, along with an increase in H_2O_2 levels, collectively indicating elevated oxidative stress ($p < 0.05$). This finding aligns with a previous study demonstrating that prolonged MV triggers oxidative stress and causes diaphragmatic damage in rats [29]. Furthermore, in the MV group with increased oxidative stress, MMP decreased in response to oxidative stress induced by elevated ROS.

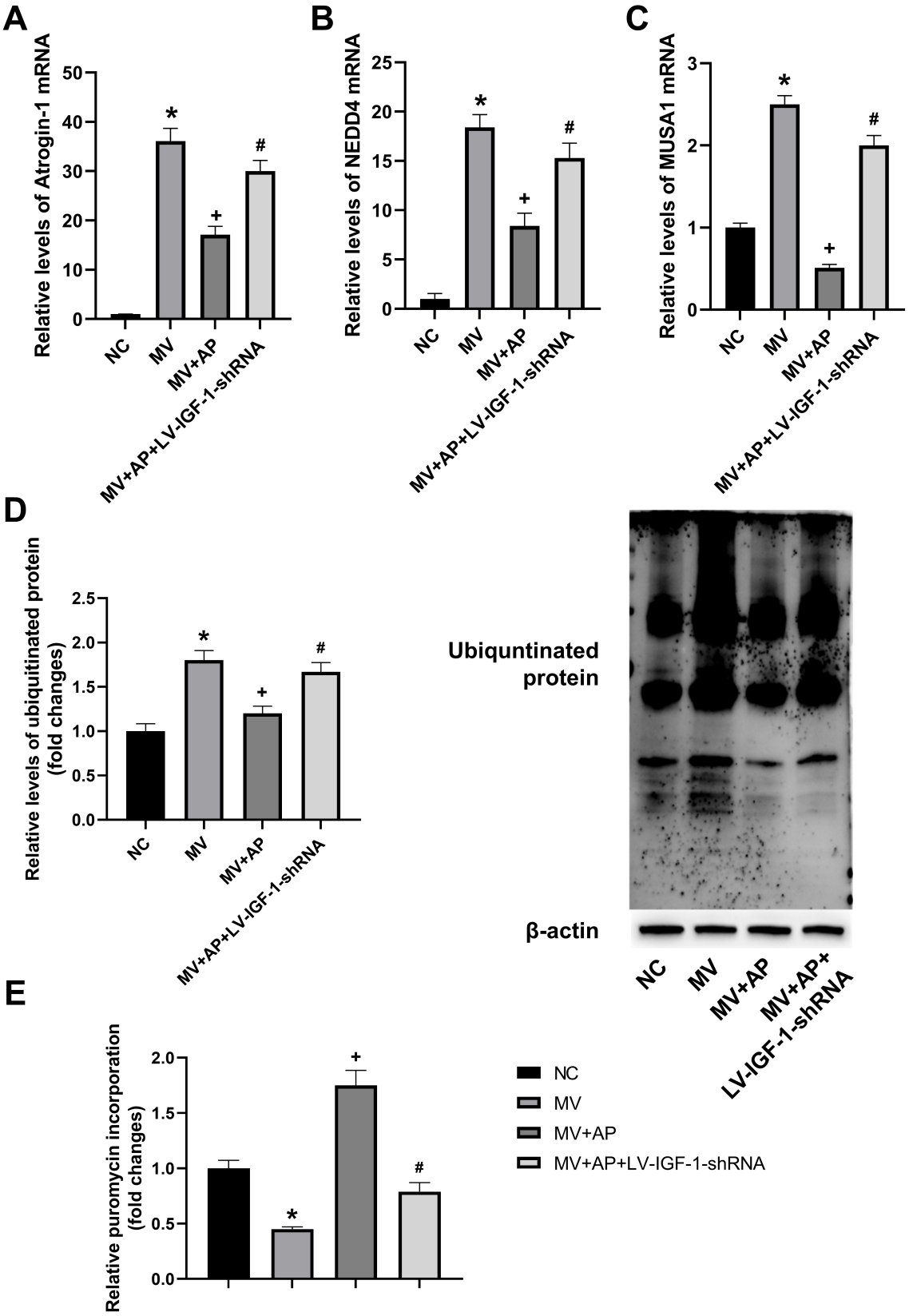

Fig. 6. AP suppresses protein degradation and promotes protein synthesis in diaphragmatic muscles. The mRNA expression levels of (A) Atrogin-1, (B) *NEDD4*, and (C) *MUSA1* in diaphragms. (D) Ubiquitinated protein levels in diaphragms. (E) The levels of puromycin in newly synthesized protein. N = 10. *$p < 0.05$ compared with the NC group. $^{+}p < 0.05$ compared with the MV group. $^{\#}p < 0.05$ compared with MV+AP group.

The genes *DRP1* and *MFN2* play essential roles in mitochondrial fission and fusion, respectively, influencing muscle atrophy through disrupted mitochondrial stability and accelerated mitophagy [30]. Notably, after MV treatment in patients, abnormal mitochondrial morphology, such as fission fragmentation, occurs immediately, demonstrating MV-induced mitophagy [31]. In this study, MV treatment increased the expression of fission-associated DRP1 expression and decreased fusion-associated *MFN2* expression, indicating altered mitochondrial dynamics caused by MV. The MV-induced increase in fission and decrease in fusion accelerated mitochondrial autophagy, contributing to VIDD.

The PINK1/Parkin pathway is crucial for regulating mitophagy [32]. In healthy mitochondria, PINK1 levels remain low as it is degraded by the PARL protein, and Parkin remains inactive due to self-suppression [33]. In damaged mitochondria, activated PINK1 phosphorylates and activates Parkin, leading to the formation of mitochondrial autophagosomes and inducing mitophagy. In this study, the MV-induced increase in PINK1 and Parkin expression indicated that MV induces mitophagy in the diaphragm.

It has been established that mitochondrial dysfunction promotes muscle atrophy through pathways associated with catabolism, and preventing diaphragmatic mitochondria from emitting ROS is protective against diaphragmatic weakness [34]. The results of this study indicate that AP treatment can reverse increased oxidative stress and mitochondrial dysfunction caused by MV when the IGF-1-FOXO1-MURF1 pathway is successfully activated. This suggests that AP can improve VIDD by ameliorating oxidative stress, mitochondrial dysfunction, and muscle weakness.

Previous studies have demonstrated that attenuated apoptosis in skeletal muscle fibers facilitates the improvement of myofiber size, and apoptosis is also involved in the muscle wasting of respiratory muscles [35]. It has been reported that oxidative stress can activate the catabolic pathway of apoptosis, which underlies VIDD. High levels of ROS can lead to cytoskeletal protein degradation, resulting in the disruption of sarcomeres and impairment of muscle force generation [36,37]. Moreover, the imbalance between protein degradation and synthesis causes muscle atrophy, resulting in muscle mass loss, disability, and weakness [38].

In the present study, apoptosis and protein degradation increased, and the rate of protein synthesis decreased in the MV group. However, all these developments that could lead to atrophy were reversed by AP administration, with no blockage of the IGF-1-FOXO1-MURF1 pathway.

Conclusions

In this study, MV treatment-induced symptoms of VIDD in rats. However, administration of AP was found to reverse these changes, including decreased contractility, reduced CSAs of muscle fibers, increased oxidative stress, impaired mitochondrial stability, heightened apoptosis and protein degradation, and decreased rates of protein synthesis. Furthermore, the observed disruption of the activation of the IGF-1-FOXO1-MURF1 pathway was found to nullify the effects of AP administration. Therefore, we conclude that AP is capable of protecting diaphragm skeletal muscle from atrophy and weakness by targeting the IGF-1-FOXO1-MURF1 pathway, demonstrating its potential for ameliorating VIDD.

Availability of Data and Materials

Data to support the findings of this study are available on reasonable request from the corresponding authors.

Author Contributions

LY and XJ contributed to the study concept and design. JT, SF, and WD contributed to the acquisition of data. LY and XJ performed the statistical analysis. JT was involved in the interpretation of the data. All authors contributed to editorial changes in the manuscript. All authors read and approved the final manuscript. All authors have participated sufficiently in the work to take public responsibility for appropriate portions of the content and agreed to be accountable for all aspects of the work in ensuring that questions related to its accuracy or integrity.

Ethics Approval and Consent to Participate

This experiment was approved by the Ethics Committee of Wuhan University (approval No. ZN2022057).

Acknowledgment

Not applicable.

Funding

This research was funded by Hubei Province health and family planning scientific research project (No: WJ2023F046); Wuhan Science and Technology Bureau knowledge innovation project (No: 2023020201010191).

Conflict of Interest

The authors declare no conflict of interest.

References

[1] Zambelli V, Murphy EJ, Delvecchio P, Rizzi L, Fumagalli R, Rezoagli E, *et al*. Treatment with levosimendan in an experimental model of early ventilator-induced diaphragmatic dysfunction. Drug Target Insights. 2023; 17: 39–44.

[2] Lentz S, Roginski MA, Montrief T, Ramzy M, Gottlieb M, Long B. Initial emergency department mechanical ventilation strategies for COVID-19 hypoxemic respiratory failure and ARDS.

The American Journal of Emergency Medicine. 2020; 38: 2194–2202.

[3] Fan C, Qi B, Chen C. Current views of the Pediatric Intensive Care Unit. Minerva Pediatrica. 2019; 71: 539–543.

[4] Dres M, Demoule A. Monitoring diaphragm function in the ICU. Current Opinion in Critical Care. 2020; 26: 18–25.

[5] Molina Peña ME, Sánchez CM, Rodríguez-Triviño CY. Physiopathological mechanisms of diaphragmatic dysfunction associated with mechanical ventilation. Revista Espanola De Anestesiologia Y Reanimacion. 2020; 67: 195–203.

[6] Pham T, Heunks L, Bellani G, Madotto F, Aragao I, Beduneau G, *et al*. Weaning from mechanical ventilation in intensive care units across 50 countries (WEAN SAFE): a multicentre, prospective, observational cohort study. The Lancet. Respiratory Medicine. 2023; 11: 465–476.

[7] Wang P, Zhou X, Li G, Ma H, Liu R, Zhao Y. Altered expression of microRNAs in the rat diaphragm in a model of ventilator-induced diaphragm dysfunction after controlled mechanical ventilation. BMC Genomics. 2021; 22: 671.

[8] Miao Y, Zhou Y, Zhao S, Liu W, Wang A, Zhang Y, *et al*. Comparative efficacy and safety of caffeine citrate and aminophylline in treating apnea of prematurity: A systematic review and meta-analysis. PloS One. 2022; 17: e0274882.

[9] Suneby Jagers JV, Ji M, Rothwell B, Easton PA. Aminophylline increases parasternal muscle action in awake canines. Pulmonary Pharmacology & Therapeutics. 2019; 56: 1–7.

[10] Bin Y, Xiao Y, Huang D, Ma Z, Liang Y, Bai J, *et al*. Theophylline inhibits cigarette smoke-induced inflammation in skeletal muscle by upregulating HDAC2 expression and decreasing NF-κB activation. American Journal of Physiology. Lung Cellular and Molecular Physiology. 2019; 316: L197–L205.

[11] Balashova L, Bykovskaya S, Korobova L, Kuznetsova Y, Kantardgy E, Mukhin V, *et al*. Immunological outcomes in infants with ROP after dexamethasone and aminophylline. Clinical and Experimental Pharmacology & Physiology. 2020; 47: 1368–1373.

[12] Yoshida T, Delafontaine P. Mechanisms of IGF-1-Mediated Regulation of Skeletal Muscle Hypertrophy and Atrophy. Cells. 2020; 9: 1970.

[13] Li J, Hu Y, Li J, Wang H, Wu H, Zhao C, *et al*. Loss of MuRF1 in Duroc pigs promotes skeletal muscle hypertrophy. Transgenic Research. 2023; 32: 153–167.

[14] Zhang H, Chi M, Chen L, Sun X, Wan L, Yang Q, *et al*. Linalool Prevents Cisplatin Induced Muscle Atrophy by Regulating IGF-1/Akt/FoxO Pathway. Frontiers in Pharmacology. 2020; 11: 598166.

[15] Cui C, Han S, Shen X, He H, Chen Y, Zhao J, *et al*. ISLR regulates skeletal muscle atrophy via IGF1-PI3K/Akt-Foxo signaling pathway. Cell and Tissue Research. 2020; 381: 479–492.

[16] Amponsah SK, Opuni KFM, Antwi KA, Kunkpeh VP. Effect of aminophylline on the pharmacokinetics of amikacin in Sprague-Dawley rats. Journal of Infection in Developing Countries. 2019; 13: 251–254.

[17] Lellouche F, Dionne S, Simard S, Bussières J, Dagenais F. High tidal volumes in mechanically ventilated patients increase organ dysfunction after cardiac surgery. Anesthesiology. 2012; 116: 1072–1082.

[18] Ravi V, Jain A, Mishra S, Sundaresan NR. Measuring Protein Synthesis in Cultured Cells and Mouse Tissues Using the Non-radioactive SUnSET Assay. Current Protocols in Molecular Biology. 2020; 133: e127.

[19] Yong H, Zhou Y, Ye W, Li T, Wu G, Chen J, *et al*. PINK1/Parkin-mediated mitophagy in mechanical ventilation-induced diaphragmatic dysfunction. Therapeutic Advances in Respiratory Disease. 2021; 15: 1753466621998246.

[20] Hyatt HW, Powers SK. Disturbances in Calcium Homeostasis Promotes Skeletal Muscle Atrophy: Lessons From Ventilator-Induced Diaphragm Wasting. Frontiers in Physiology. 2020; 11: 615351.

[21] Ichinoseki-Sekine N, Smuder AJ, Morton AB, Hinkley JM, Mor Huertas A, Powers SK. Hydrogen sulfide donor protects against mechanical ventilation-induced atrophy and contractile dysfunction in the rat diaphragm. Clinical and Translational Science. 2021; 14: 2139–2145.

[22] Hemmi S, Kurokawa K, Nagai T, Asano A, Okamoto T, Murakami T, *et al*. Influence of placement sites of the active recording electrode on CMAP configuration in the trapezius muscle. Clinical Neurophysiology Practice. 2018; 3: 54–58.

[23] Leermakers PA, Skov M, Riisager A, Nielsen OB, Pedersen TH. Alterations in fast-twitch muscle membrane conductance regulation do not explain decreased muscle function of $SOD1^{G93A}$ rats. Muscle & Nerve. 2021; 64: 755–764.

[24] Zong Y, Lu Z, Chen M, Li X, Stampas A, Deng L, *et al*. CMAP Scan Examination of the First Dorsal Interosseous Muscle After Spinal Cord Injury. IEEE Transactions on Neural Systems and Rehabilitation Engineering: a Publication of the IEEE Engineering in Medicine and Biology Society. 2021; 29: 1199–1205.

[25] Tang H, Shrager JB. The Signaling Network Resulting in Ventilator-induced Diaphragm Dysfunction. American Journal of Respiratory Cell and Molecular Biology. 2018; 59: 417–427.

[26] Eyenga P, Roussel D, Rey B, Ndille P, Teulier L, Eyenga F, *et al*. Mechanical ventilation preserves diaphragm mitochondrial function in a rat sepsis model. Intensive Care Medicine Experimental. 2021; 9: 19.

[27] Smuder AJ, Sollanek KJ, Nelson WB, Min K, Talbert EE, Kavazis AN, *et al*. Crosstalk between autophagy and oxidative stress regulates proteolysis in the diaphragm during mechanical ventilation. Free Radical Biology & Medicine. 2018; 115: 179–190.

[28] Jin Z, Chang B, Wei Y, Yang Y, Zhang H, Liu J, *et al*. Curcumin exerts chondroprotective effects against osteoarthritis by promoting AMPK/PINK1/Parkin-mediated mitophagy. Biomedicine & Pharmacotherapy. 2022; 151: 113092.

[29] Li LF, Yu CC, Wu HP, Chu CM, Huang CY, Liu PC, *et al*. Reduction in Ventilation-Induced Diaphragmatic Mitochondrial Injury through Hypoxia-Inducible Factor 1α in a Murine Endotoxemia Model. International Journal of Molecular Sciences. 2022; 23: 1083.

[30] Peyravi A, Yazdanpanahi N, Nayeri H, Hosseini SA. The effect of endurance training with crocin consumption on the levels of MFN2 and DRP1 gene expression and glucose and insulin indices in the muscle tissue of diabetic rats. Journal of Food Biochemistry. 2020; 44: e13125.

[31] Joelsson JP, Asbjarnarson A, Sigurdsson S, Kricker J, Valdimarsdottir B, Thorarinsdottir H, *et al*. Ventilator-induced lung injury results in oxidative stress response and mitochondrial swelling in a mouse model. Laboratory Animal Research. 2022; 38: 23.

[32] Yin J, Guo J, Zhang Q, Cui L, Zhang L, Zhang T, *et al*. Doxorubicin-induced mitophagy and mitochondrial damage is associated with dysregulation of the PINK1/parkin pathway. Toxicology *in Vitro*: an International Journal Published in Association with BIBRA. 2018; 51: 1–10.

[33] Hu J, Liu T, Fu F, Cui Z, Lai Q, Zhang Y, *et al*. Omentin1 ameliorates myocardial ischemia-induced heart failure via SIRT3/FOXO3a-dependent mitochondrial dynamical homeostasis and mitophagy. Journal of Translational Medicine. 2022; 20: 447.

[34] Zhang YY, Gu LJ, Huang J, Cai MC, Yu HL, Zhang W, *et al*. CKD autophagy activation and skeletal muscle atrophy-a preliminary study of mitophagy and inflammation. European Journal of Clinical Nutrition. 2019; 73: 950–960.

[35] Salazar-Degracia A, Granado-Martínez P, Millán-Sánchez A, Tang J, Pons-Carreto A, Barreiro E. Reduced lung cancer burden by selective immunomodulators elicits improvements in muscle proteolysis and strength in cachectic mice. Journal of Cellular Physiology. 2019; 234: 18041–18052.

[36] Xiang Y, Dai J, Li Y, You Z, Zhang J, Huang X, *et al*. ROS-activated CXCR2^{+} neutrophils recruited by CXCL1 delay denervated skeletal muscle atrophy and undergo P53-mediated apoptosis. Experimental & Molecular Medicine. 2022; 54: 1011–1023.

[37] Chen X, Zhang Y, Jiang S, Huang S. Maduramicin induces apoptosis through ROS-PP5-JNK pathway in skeletal myoblast cells and muscle tissue. Toxicology. 2019; 424: 152239.

[38] Wang Y, Liu Q, Quan H, Kang SG, Huang K, Tong T. Nutraceuticals in the Prevention and Treatment of the Muscle Atrophy. Nutrients. 2021; 13: 1914.